

# Thermal Conductivity of Neutrons in Neutron Star Cores

D.A. Baiko<sup>1</sup>, P. Haensel<sup>2</sup> and D.G. Yakovlev<sup>1,3</sup>

<sup>1</sup> A.F. Ioffe Physical Technical Institute, Politekhnikeskaya 26, 194021, St.Petersburg, Russia

<sup>2</sup> N. Copernicus Astronomical Center, Bartycka 18, 00-716, Warsaw, Poland

<sup>3</sup> Institute for Theoretical Physics, University of California, Santa Barbara, CA 93106, USA  
e-mail: baiko@mail.rit.edu, haensel@camk.edu.pl, yak@astro.ioffe.rssi.ru

Received; accepted

**Abstract.** The diffusive thermal conductivity of neutrons in dense matter [ $\rho \sim (1 - 8) \times 10^{14}$  g cm<sup>-3</sup>] of neutron star cores is calculated. The contribution from neutron–neutron and neutron–proton collisions is taken into account. We use the transition probabilities calculated for symmetric dense nucleon matter on the basis of the Dirac–Brueckner approach to the in-medium effects and the Bonn model of bare nucleon–nucleon interaction. The diffusive thermal conductivity of neutrons in the presence of neutron and proton superfluidities is analyzed in a microscopic manner; the effects of superfluidity are shown to be significant. The low temperature behavior of the thermal conductivity appears to be extremely sensitive to the relation between critical temperatures of neutrons and protons. The results are fitted by simple analytic expressions. In combination with the formulae for the electron and muon thermal conductivities, obtained earlier, the present expressions provide a realistic description of the full diffusive thermal conductivity in the neutron star cores for normal and various superfluid phases.

**Key words.** Stars: neutron – dense matter – conduction

## 1. Introduction

We study the thermal conductivity of neutrons in the neutron star cores, in the density range  $\rho \sim (0.5 - 3)\rho_0$ , where  $\rho_0 = 2.8 \times 10^{14}$  g cm<sup>-3</sup> is the normal nuclear density. The problem is important for numerical simulations of cooling of young neutron stars, before internal thermal equilibrium is achieved. The non-relaxed stage lasts 10 – 100 yr (Van Riper, 1991, Umeda et al., 1993, Lattimer et al., 1994) depending on the model of dense matter.

At densities close to  $\rho_0$ , neutron star matter is expected to consist mostly of neutrons ( $n$ ), with a small (a few percent) admixture of protons ( $p$ ), electrons ( $e$ ) and, at densities where the electron Fermi energy exceeds the muon rest energy, also of muons ( $\mu$ ). In what follows, we adopt this  $npe\mu$  model of neutron star matter within the considered density range. At higher  $\rho$  other particles may appear, first of all hyperons (e.g., Balberg et al. 1999). We discuss briefly thermal conductivity of hyperonic matter in Sect. 4.

Numerical simulations of neutron star cooling traditionally employ the thermal conductivity obtained by Flowers & Itoh (1979, 1981) about 20 years ago. These authors proposed an analytic fit valid for non-superfluid matter, and discussed qualitatively the effects of nucleon

superfluidity. It is now generally recognized that the neutron star cores can be in a superfluid state (see, e.g., Pines, 1991, Page & Applegate, 1992, Yakovlev et al., 1999). Moreover, Flowers & Itoh (1979, 1981) calculated the thermal conductivity for one specific model of dense matter which is inconvenient as the equation of state of neutron star cores is generally unknown. The thermal conductivity of the neutron star cores was analyzed also by Wambach et al. (1993) and by Sedrakian et al. (1994), again for some selected models of dense matter and neglecting the superfluidity effects. Thus, it is desirable to obtain new expressions which apply to various models of matter and take into account nucleon superfluidity. In contrast to the studies of Flowers & Itoh (1979), Wambach et al. (1993), Sedrakian et al. (1994), we consider the effects of nucleon superfluidity in a microscopic manner by evaluating the diffusive thermal conductivity of neutrons in superfluid matter.

The main heat carriers in the neutron star cores are neutrons (the most abundant particles) as well as electrons and muons which have large mean free paths since they experience only relatively weak, Coulomb interactions. The thermal conductivity of protons is small (Flowers & Itoh, 1979) and can be neglected. The heat conduction of electrons and muons is limited by Coulomb collisions with  $e$ ,  $p$  and  $\mu$ , while that of neutrons is limited by their col-

lisions with  $n$  and  $p$  due to the strong nucleon–nucleon interaction. Accordingly, the neutron transport is almost independent of the electron and muon one, and can be studied separately. This property was proved by Flowers & Itoh (1979) who decoupled the overall heat–conduction equations into two blocks describing the conductivities of neutrons and electrons.

The thermal conductivity of electrons and muons was reconsidered by Gnedin & Yakovlev (1995) who obtained simple expressions valid for a wide class of models of superfluid and non-superfluid matter. In the present article, we reanalyze the thermal conduction of neutrons utilizing some new developments in the nucleon–nucleon interaction theory. In combination with the results of Gnedin & Yakovlev (1995), this describes the diffusive heat transport in not too dense neutron star cores.

In the presence of neutron superfluidity there may be another channel of heat transport, the so-called convective counterflow of normal component of matter with respect to superfluid one. This mechanism is known to be extremely effective in superfluid helium (e.g., Tilley & Tilley, 1990) but in the case of neutron star matter the situation is more complicated. The related effects require separate study and will not be considered here.

## 2. General Formalism

Consider a neutron star core at densities  $\rho$  from about  $0.5\rho_0$  to  $3\rho_0$ . The lower limit corresponds to the core–crust transition (Lorenz et al., 1993, Pethick & Ravenhall, 1995), while the upper limit is the typical central density of a not too massive star. We treat neutrons as non-relativistic particles and do not study higher  $\rho$  where they become mildly relativistic.

To calculate the neutron conductivity, it is sufficient to consider the nucleon component of matter. In the density range of study, typical Fermi energy of neutrons changes from a few ten to a few hundred MeV (e.g., Shapiro & Teukolsky, 1983). Fermi energy of protons varies from several MeV to a few tens of MeV. Since the temperature in the cores of cooling neutron stars is typically well below  $10^{10}$  K (1 MeV), both neutrons and protons form strongly degenerate Fermi liquids.

In the limit of strong degeneracy transport properties of a nucleon liquid can be described using the concept of *quasiparticles*. In the present section, we restrict ourselves to the case of *normal* nucleon liquids (the effects of nucleon superfluidity will be considered in Sect. 3). Landau theory of normal Fermi liquids enables one to identify the low temperature properties of a strongly interacting real system with those of a dilute gas of weakly interacting elementary excitations — the nucleon quasiparticles (a detailed description of the theory and its applications can be found in Baym & Pethick, 1991). This formalism can be used effectively only for describing small macroscopic deviations of the real system from its ground state. A crucial feature of the Landau Fermi–liquid theory is the inclusion of the quasiparticle interaction. The kinetics of quasipar-

ticles can be described including only binary quasiparticle collisions. We are interested in the collisions of neutron quasiparticles with neutron and proton quasiparticles. In the calculation of the neutron thermal conductivity protons will be considered as scatterers.

### 2.1. Kinetic equation

The distribution function  $F_n$  of neutron quasiparticles satisfies the Landau kinetic equation (e.g., Baym & Pethick, 1991) which describes motion of a given quasiparticle in a self-consistent field of its neighbors. However, a proper linearization reduces the Landau equation to a Boltzmann-like equation. The linearized expression for the quasiparticle thermal flux density also takes its standard form. This enables us to use the expressions familiar from the kinetics of dilute gases (e.g., Ziman, 1960). The thermal flux density of neutrons is

$$\mathbf{q}_n = \frac{2}{(2\pi)^3} \int d\mathbf{k}_n (\epsilon_n - \mu_n) \mathbf{v}_n F_n \equiv -\kappa_n \nabla T, \quad (1)$$

where  $\mathbf{k}_n$ ,  $\mathbf{v}_n$ ,  $\epsilon_n$ ,  $\mu_n$  are the neutron wave-vector, velocity, energy, and chemical potential, respectively;  $\kappa_n$  is the neutron thermal conductivity to be determined, and  $T$  is the temperature. In the presence of a weak temperature gradient, the Boltzmann equation reads

$$\mathbf{v}_n \cdot \nabla F_n = I_{nn} + I_{np}, \quad (2)$$

where  $I_{nn}$  and  $I_{np}$  are the  $nn$  and  $np$  collision integrals:

$$\begin{aligned} I_{12} = & \frac{V^3}{(2\pi)^9 (1 + \delta_{12})} \int \int \int d\mathbf{k}'_1 d\mathbf{k}_2 d\mathbf{k}'_2 \\ & \times \sum_{\sigma'_1 \sigma_2 \sigma'_2} \mathcal{P}_{12} [F'_1 F'_2 (1 - F_1) (1 - F_2) \\ & - F_1 F_2 (1 - F'_1) (1 - F'_2)]. \end{aligned} \quad (3)$$

The non-primed quantities refer to the particles before a collision event, while the primed ones refer to the particles after the collision,  $\sigma$  denotes the spin state, and  $\mathcal{P}_{12}$  is the differential transition rate. The rates of direct and inverse processes are equal due to detailed balancing. The term  $\delta_{12}$  serves to avoid double counting of the final states in the case of  $nn$  collisions;  $V$  is the normalization volume.

Since the protons are treated as scatterers (but not the heat carriers) their distribution function coincides with the equilibrium Fermi–Dirac distribution  $f(\epsilon)$ :

$$\begin{aligned} F_p &= f_p \equiv f(\epsilon_p), \\ f(\epsilon) &\equiv \left[ 1 + \exp\left(\frac{\epsilon - \mu}{T}\right) \right]^{-1}. \end{aligned} \quad (4)$$

The neutron distribution can be written as

$$F_n = f_n - \Phi_n \frac{\partial f_n}{\partial \epsilon_n}, \quad (5)$$

where  $f_n = f(\epsilon_n)$ , and  $\Phi_n = \Phi_n(\epsilon_n)$  describes the small deviation of the distribution function from the equilibrium

one. This correction is known (Ziman, 1960) to have the form

$$\Phi_n = -\tau_n (\epsilon_n - \mu_n) \frac{\mathbf{v}_n \cdot \nabla T}{T}, \quad (6)$$

where  $\tau_n$  is the effective relaxation time of neutrons which is generally a complicated function of the energy parameter  $(\epsilon_n - \mu_n)/T$ . However, while solving the transport equation, we will rely on the variational approach and choose the simplest trial function consistent with a symmetry requirement imposed on  $\Phi_n$ . This corresponds to  $\tau_n$  independent of energy.

Notice that the thermal conductivity can be calculated exactly using the formalism developed by Sykes & Brooker (1970), Højgaard Jensen et al. (1968), Flowers & Itoh (1979), and Anderson et al. (1987). In Sect. 2.7 we discuss the corrections to our results which follow from the exact theory.

## 2.2. Relaxation time

Inserting  $F_n$  from Eqs. (5) and (6) into (1) we have

$$\kappa_n = \frac{\pi^2 T n_n \tau_n}{3m_n^*}, \quad (7)$$

where  $n_n$  and  $m_n^*$  are the neutron number density and effective mass, respectively. The relaxation time  $\tau_n$  has to be determined from Eq. (2).

Following the standard procedure we linearize the kinetic equation with respect to the small nonequilibrium correction  $\Phi_n$  to the Fermi–Dirac distribution. The linearized left-hand side of Eq. (2) is

$$\mathbf{v}_n \cdot \nabla F_n \approx \mathbf{v}_n \cdot \nabla f_n = \frac{\partial f_n}{\partial T} \mathbf{v}_n \cdot \nabla T. \quad (8)$$

Inserting Eqs. (4) and (5) into (3), we arrive at the linearized collision integrals

$$I_{12} = \frac{\tau_n V^3 \nabla T}{(2\pi)^9 (1 + \delta_{12}) T^2} \int \int \int d\mathbf{k}'_1 d\mathbf{k}_2 d\mathbf{k}'_2 f_1 f_2 \times (1 - f'_1)(1 - f'_2) \sum_{\sigma'_1 \sigma_2 \sigma'_2} \mathcal{P}_{12} \mathbf{V}_{12}, \quad (9)$$

where  $\mathbf{V}_{nn} = (\epsilon_1 - \mu_n) \mathbf{v}_1 + (\epsilon_2 - \mu_n) \mathbf{v}_2 - (\epsilon'_1 - \mu_n) \mathbf{v}'_1 - (\epsilon'_2 - \mu_n) \mathbf{v}'_2$  and  $\mathbf{V}_{np} = (\epsilon_1 - \mu_n) \mathbf{v}_1 - (\epsilon'_1 - \mu_n) \mathbf{v}'_1$ .

Let us multiply the linearized Boltzmann equation by  $d\mathbf{k}_n (2\pi)^{-3} (\epsilon_n - \mu_n) \mathbf{v}_n$ , integrate over  $d\mathbf{k}_n$  and sum over the neutron spin states  $\sigma_n$ . From the left-hand side of the Boltzmann equation we obtain

$$C_n = \sum_{\sigma_n} \int \frac{d\mathbf{k}_n}{(2\pi)^3} (\epsilon_n - \mu_n) v_n^2 \frac{\partial f_n}{\partial T} = \frac{\pi^2 T n_n}{m_n^*}. \quad (10)$$

On the right-hand side, we have  $\pi^2 \tau_n T n_n (\nu_{nn} + \nu_{np}) / m_n^*$ , where we have introduced the effective  $nn$  and  $np$  collision frequencies  $\nu_{nn}$  and  $\nu_{np}$ :

$$\nu_{12} = \frac{m_n^* V^3}{(2\pi)^{12} \pi^2 T^3 n_n (1 + \delta_{12})} \int \int \int \int d\mathbf{k}_1 d\mathbf{k}'_1$$

$$\times d\mathbf{k}_2 d\mathbf{k}'_2 \sum_{\sigma_1 \sigma'_1 \sigma_2 \sigma'_2} \mathcal{P}_{12} f_1 f_2 \times (1 - f'_1)(1 - f'_2) (\epsilon_1 - \mu_n) \mathbf{V}_{12} \cdot \mathbf{v}_1. \quad (11)$$

Now the relaxation time is:

$$\tau_n = \frac{1}{\nu_{nn} + \nu_{np}}. \quad (12)$$

The differential transition rate summed over initial and final spin states can be written as:

$$\sum_{\sigma_1 \sigma'_1 \sigma_2 \sigma'_2} \mathcal{P}_{12} = 4 \frac{(2\pi)^4}{\hbar V^3} \delta(\epsilon_1 + \epsilon_2 - \epsilon'_1 - \epsilon'_2) \times \delta(\mathbf{k}_1 + \mathbf{k}_2 - \mathbf{k}'_1 - \mathbf{k}'_2) \mathcal{Q}_{12}, \quad (13)$$

where  $\mathcal{Q}_{12} = (1/4) \sum_{\text{spins}} |M_{12}|^2$  is the squared matrix element averaged over initial and summed over final spin states. Since no specific spin orientations are involved,  $\mathcal{Q}_{12}$  can depend only on the scalar combinations of the momentum transfers  $\mathbf{q} = \mathbf{k}'_2 - \mathbf{k}_2$  and  $\mathbf{q}' = \mathbf{k}'_2 - \mathbf{k}_1$ , that is on  $q$ ,  $q'$  and  $(\mathbf{q} \cdot \mathbf{q}')$ . In our case, the scalar product  $(\mathbf{q} \cdot \mathbf{q}')$  is zero (see Sect. 2.3). Therefore,  $\mathcal{Q}_{12}$  is a function of  $q$  and  $q'$  alone.

## 2.3. Energy–angular decomposition

Since neutrons and protons are strongly degenerate, we can use the conventional energy–angular decomposition while evaluating the collision frequencies  $\nu_{12}$ . The main contribution to the integrals comes from narrow vicinities of  $k$  near  $k = k_F$  in which  $\hbar v_F |k - k_F| \lesssim T$  (in this case  $k_F$  and  $v_F$  are a particle Fermi wavenumber and velocity). In these regions, we can introduce convenient momentum variable  $\xi = \hbar v_F (k - k_F)$  with  $d\xi = d\epsilon$ . Then we can replace integration over  $k$  by that over  $\xi$  extending the integration limits to  $\pm\infty$ , since the domains of integration outside the indicated vicinities give exponentially small contributions. Thus  $\hbar^2 d\mathbf{k} = k_F m^* d\xi d\Omega$ , where  $d\Omega$  is a solid angle element in the direction of  $\mathbf{k}$ . Moreover, we can place the particle wave vectors  $\mathbf{k}$  at the appropriate Fermi surfaces in all smooth functions of the momenta. Consequently, the expressions for  $\nu_{12}$  are decomposed into sums of products containing decoupled integrations over angles  $d\Omega$  and momentum (energy) variables  $d\xi$  of all colliding particles. Placing all the particle wave vectors on their Fermi surfaces, one can easily verify that the momentum transfers  $\mathbf{q}$  and  $\mathbf{q}'$  are perpendicular, as already mentioned in Sect. 2.2. Using the well-known symmetry properties of the energy integrals and the relations which come from momentum conservation for the particles at their Fermi surfaces in the angular integrals, after standard transformations (e.g., Ziman, 1960) we obtain

$$\nu_{12} = \frac{3m_1^* k_{F1} m_2^* k_{F2}^2}{2^6 \pi^8 T^3 \hbar^7 (1 + \delta_{12})} \times \int \int \int \int_{-\infty}^{+\infty} d\xi_1 d\xi'_1 d\xi_2 d\xi'_2 f_1 f_2 \times (1 - f'_1)(1 - f'_2) \delta(\epsilon_1 + \epsilon_2 - \epsilon'_1 - \epsilon'_2)$$

$$\begin{aligned} & \times \int \int \int \int d\Omega_1 d\Omega'_1 d\Omega_2 d\Omega'_2 \delta(\mathbf{k}_1 + \mathbf{k}_2 - \mathbf{k}'_1 - \mathbf{k}'_2) \\ & \times \mathcal{Q}_{12}(q, q') (\xi_1^2 - \xi_1 \xi'_1 A_{12}), \end{aligned} \quad (14)$$

where  $A_{nn} = 3 - (q^2 + q'^2)/k_{\text{Fn}}^2$ ,  $A_{np} = 1 - q^2/(2k_{\text{Fn}}^2)$ . These expressions contain two energy integrals  $J_1$  and  $J_2$  of the form

$$\begin{aligned} J_\alpha &= \int \int \int \int_{-\infty}^{+\infty} d\xi_1 d\xi'_1 d\xi_2 d\xi'_2 \delta(\epsilon_1 + \epsilon_2 - \epsilon'_1 - \epsilon'_2) \\ & \times f_1 f_2 (1 - f'_1) (1 - f'_2) (\epsilon_1 - \mu_n) B_\alpha, \end{aligned} \quad (15)$$

with  $B_1 = \epsilon_1 - \mu_1$  and  $B_2 = \epsilon'_1 - \mu_1$ . They may be evaluated analytically:

$$J_1 = 3 J_2 = \frac{2}{5} \pi^4 T^5. \quad (16)$$

Thus we arrive at the equations which contain the angular integration

$$\begin{aligned} \nu_{12} &= \frac{16\pi^5 m_1^* m_2^{*2} k_{\text{Fn}}^2 T^2}{5 k_{\text{Fn}} (2\pi)^9 \hbar^7 (1 + \delta_{12})} \int \int \int \int d\Omega_1 d\Omega'_1 d\Omega_2 d\Omega'_2 \\ & \times \delta(\mathbf{k}_1 + \mathbf{k}_2 - \mathbf{k}'_1 - \mathbf{k}'_2) \mathcal{Q}_{12}(q, q') C_{12}, \end{aligned} \quad (17)$$

where  $C_{nn} = q^2 + q'^2$  and  $C_{np} = 2k_{\text{Fn}}^2 + (q^2/2)$ .

#### 2.4. Angular integration

It is clear that the integrands depend only on the relative orientations of the particle momenta. Then we can immediately integrate over the orientations of the momentum of the first particle before the scattering, and over the azimuthal angle which specifies the momentum of the second colliding particle with respect to the first one. This yields an overall factor  $8\pi^2$ . Let  $\theta$  be an angle between the momenta of colliding particles before the scattering, and  $\theta_1, \theta_2, \phi_1, \phi_2$  be the polar and azimuthal angles of the particles after the scattering in a coordinate frame with  $z$  axis along  $\mathbf{k}_1$  and  $x$  axis placed in a  $(\mathbf{k}_1 \mathbf{k}_2)$ -plane. Accordingly,

$$\sin \theta_1 d\theta_1 = \frac{q dq}{k_{\text{F1}}^2}, \quad \sin \theta_2 d\theta_2 = \frac{q' dq'}{k_{\text{F1}} k_{\text{F2}}}, \quad (18)$$

and the integration over  $\theta, \phi_1, \phi_2$  is performed with aid of the  $\delta$ -function:

$$\begin{aligned} & \frac{k_{\text{F2}}}{k_{\text{F1}}} \int \int \int \sin \theta d\theta d\phi_1 d\phi_2 \delta(\mathbf{k}_1 + \mathbf{k}_2 - \mathbf{k}'_1 - \mathbf{k}'_2) \\ &= \frac{4}{qq' \sqrt{A^2 - q^2}}, \end{aligned} \quad (19)$$

where

$$A^2 = \frac{1}{q'^2} [4k_{\text{F1}}^2 k_{\text{F2}}^2 - (k_{\text{F1}}^2 + k_{\text{F2}}^2 - q'^2)^2], \quad (20)$$

$$q \leq A, |k_{\text{F1}} - k_{\text{F2}}| \leq q' \leq (k_{\text{F1}} + k_{\text{F2}}).$$

Inserting (19) into (17) we can express  $\nu_{nn}$  and  $\nu_{np}$  in a unified manner

$$\nu_{12} = \frac{64m_1^* m_2^{*2} k_{\text{B}}^2 T^2}{5m_N^2 \hbar^3} S_{12}. \quad (21)$$

Here, we introduce the convenient quantities of dimension of a cross section ( $\text{cm}^2$ ):  $S_{nn} \equiv S_{n2}$  and  $S_{np} = S_{p1} + S_{p2}$ :

$$\begin{aligned} S_{n1} &= \frac{m_N^2}{16\pi^2 \hbar^4} \int_0^1 dx' \int_0^{\sqrt{1-x'^2}} dx \frac{1}{\sqrt{1-x^2-x'^2}} \mathcal{Q}_{nn}, \\ S_{n2} &= \frac{m_N^2}{16\pi^2 \hbar^4} \int_0^1 dx' \int_0^{\sqrt{1-x'^2}} dx \frac{x^2 + x'^2}{\sqrt{1-x^2-x'^2}} \mathcal{Q}_{nn}, \\ S_{p1} &= \frac{m_N^2}{16\pi^2 \hbar^4} \int_{0.5-x_0}^{0.5+x_0} dx' \int_0^{a(x')} dx \frac{1}{\sqrt{a^2-x^2}} \mathcal{Q}_{np}, \\ S_{p2} &= \frac{m_N^2}{16\pi^2 \hbar^4} \int_{0.5-x_0}^{0.5+x_0} dx' \int_0^{a(x')} dx \frac{x^2}{\sqrt{a^2-x^2}} \mathcal{Q}_{np}. \end{aligned} \quad (22)$$

In this case,  $x = q/(2k_{\text{Fn}})$ ,  $x' = q'/(2k_{\text{Fn}})$ ,  $x_0 = k_{\text{Fp}}/(2k_{\text{Fn}})$ ,  $a(x') = \sqrt{x_0^2 - (0.25 + x_0^2 - x'^2)^2}/x'$ ,  $m_N$  is a bare nucleon mass (we neglect the small difference between the bare neutron and proton masses). The quantity  $S_{n1}$  is not needed here but will be required in Sect. 3.

Thus we have expressed  $\nu_{12}$  through the 2D integral of the squared matrix element  $\mathcal{Q}_{12}$  over the particle momenta transfers  $q$  and  $q'$ . This integration can be performed numerically. Note that for  $nn$  collisions  $q$  varies from 0 to  $2k_{\text{Fn}}$  and scattering at arbitrary angles contributes to the integration. By contrast, in the  $np$  case  $a(x')$  does not exceed  $2x_0$  that is scattering angles larger than  $2 \arcsin(k_{\text{Fp}}/k_{\text{Fn}})$  are forbidden. We recall that, typically,  $k_{\text{Fp}} \ll k_{\text{Fn}}$ , in neutron star cores.

At this stage it is convenient to introduce the scattering cross section.

#### 2.5. Scattering cross section

The squared matrix element  $\mathcal{Q}_{12}$  determines the scattering cross section. The nucleon-nucleon cross section is more convenient for practical calculations since it has been the subject of some studies. To translate the cross section into the squared matrix element one should be careful about kinematics. We are looking for a matrix element between the quasiparticle states with certain momenta. Let us consider an idealized case, in which we can approximate nucleon quasiparticles by bare nucleons. The simplest choice would be then to equate this matrix element to that for scattering of nucleons with the same momenta in vacuum. This proceeds as follows. Let us specify, for our imaginary bare nucleons, the center-of-mass (cm) reference frame in which the total momentum of a colliding pair is zero, and the laboratory (lab) reference frame in which the initial momentum of the second particle is zero. Using standard quantum mechanics we find the familiar relations:

$$\frac{d\sigma_{12}}{d\Omega_{\text{cm}}}(\epsilon_{\text{lab}}, \theta_{\text{cm}}) = \frac{m_N^2}{16\pi^2 \hbar^4} \mathcal{Q}_{12}, \quad (23)$$

$$\cos \theta_{\text{cm}} = \frac{q'^2 - q^2}{q'^2 + q^2}, \quad (24)$$

$$\epsilon_{\text{lab}} = \frac{\hbar^2}{2m_N} (q^2 + q'^2). \quad (25)$$

In this representation, which is popular in the current literature, the cross section is a function of scattering angle in the center-of-mass frame and collision energy in the laboratory frame.

However, there exists a more involved approximation based on recent microscopic calculations of  $NN$  scattering cross sections in medium (see also Sect. 2.6). To restore the squared matrix element in this case, we again consider the two reference frames but this time for quasiparticles. The quasiparticle energy and momentum transformations which accompany a Galilean transformation from one frame to another may be found in Sect. 1.1.3 of Baym & Pethick (1991). Although the scattering angle in the center-of-mass reference frame is still given by Eq. (24), other expressions change:

$$\frac{d\sigma_{12}}{d\Omega_{\text{cm}}} = \frac{(m_1^* m_2^*)^2 (q^2 + q'^2)^{3/2} Q_{12}}{8\pi^2 \hbar^4} \times [(k_{F1}^2 m_2^* - k_{F2}^2 m_1^*) (m_2^* - m_1^*) + m_1^* m_2^* (q^2 + q'^2)]^{-1/2} \times [(q^2 + q'^2)(m_1^* + m_2^*) + (k_{F1}^2 - k_{F2}^2)(m_2^* - m_1^*)]^{-1}, \quad (26)$$

$$\epsilon_{\text{lab}} = \frac{\hbar^2}{2m_N} (q^2 + q'^2) + \frac{p_{F1}^2}{2m_N} \left( \frac{m_N}{m_1^*} - 1 \right) + \frac{p_{F2}^2}{2m_N} \left( \frac{m_N}{m_2^*} - 1 \right). \quad (27)$$

If the effective masses of colliding quasiparticles coincide, Eq. (26) reduces to a much simpler Eq. (23), with  $m^*$  in place of  $m_N$ .

## 2.6. Calculation of $S_\alpha$

For the collision energies up to 550 MeV we are interested in, the quark structure of matter is not yet pronounced, and the bare  $NN$  interaction can be described in terms of various virtual-meson-exchange processes.

Very good agreement with experimental data on the elastic  $NN$  scattering at energies up to 350 MeV is achieved using the Bonn potential model (Machleidt et al. 1987). It includes all possible diagrams which describe the exchange of  $\pi$ ,  $\rho$ ,  $\omega$ ,  $\eta$ , and  $\delta$  mesons as well as the exchange of  $2\pi$ ,  $3\pi$ ,  $\pi + \rho$  mesons and other combinations of mesons with total energy of any process up to 1 GeV. The maximum collision energy of 350 MeV is mentioned because the model does not include the inelastic channels of  $\pi$  meson creation allowed at higher energies. We do not consider matter with pion condensates, and, therefore, we do not allow for these inelastic channels.

The bare  $NN$  potential is known to be attractive at large distances and repulsive at short ones. The short-range repulsive core is extremely strong, and the Born approximation fails to describe the  $NN$  collisions of interest. Thus we use the exact transition probabilities obtained with the Bonn potential.

The differential cross sections for free nucleons have been compiled from tables presented by Li & Machleidt (1993, 1994). These authors consider *in-medium* effects but their calculations are extended to the limit of zero medium density which is the in-vacuum case. The latter cross sections are computed for laboratory energies up to 300 MeV, and the results are in nice agreement with experimental data. For convenience, we prefer to use these theoretical data rather than the experimental ones. The cross sections of the  $nn$  collisions at higher energies have been set equal to their values at 300 MeV since, according to the experimental data, the  $nn$  cross sections are almost energy-independent in this range.

The treatment of the many-body effects is complicated. For instance, Li & Machleidt (1993, 1994) performed calculations for symmetric nuclear matter as they were interested in heavy-ion collisions. The detailed calculations for arbitrary asymmetry of matter, in particular, for strongly asymmetric matter in neutron star cores have not yet been done, to our knowledge. The many-body effects turn out to be rather significant; they mainly reduce the scattering cross sections by a factor of 2–6. Although the in-medium effects can obviously be different in the symmetric and asymmetric matter, we make use of the available results to illustrate possible influence of medium on the transport properties.

We have calculated the integrals (22) using both in-medium and in-vacuum sets of the scattering cross sections obtained with the Bonn model for the values of  $k_{Fn}$  from 1.1 to 2.6 fm<sup>-1</sup> and for the values of  $k_{Fp}$  from 0.3 to 1.2 fm<sup>-1</sup> with the maximum ratio of  $k_{Fp}$  to  $k_{Fn}$  equal to 0.7. This grid certainly covers the range of possible variation of  $k_{Fn}$  and  $k_{Fp}$  for any realistic equation of state of matter at densities  $0.5\rho_0 \lesssim \rho \lesssim 3\rho_0$ . While restoring the squared matrix element from the in-medium cross sections we set  $m_n^* = m_p^* = 0.8 m_N$  in Eqs. (26) and (27).

The numerical results are fitted by simple analytic functions and written in the form

$$S_\alpha = S_\alpha^{(0)} K_\alpha, \quad (28)$$

where  $S_\alpha^{(0)}$  corresponds to scattering of bare particles, and  $K_\alpha$  describes the in-medium effects. In all these fits,  $k_{Fn}$  and  $k_{Fp}$  are expressed in fm<sup>-1</sup>.

The fit expressions for the in-vacuum integrals are

$$\begin{aligned} S_{n1}^{(0)} &= \frac{14.57}{k_{Fn}^{1.5}} \times \frac{1 - 0.0788 k_{Fn} + 0.0883 k_{Fn}^2}{1 - 0.1114 k_{Fn}} \text{ mb}, \\ S_{n2}^{(0)} &= \frac{7.880}{k_{Fn}^2} \times \frac{1 - 0.2241 k_{Fn} + 0.2006 k_{Fn}^2}{1 - 0.1742 k_{Fn}} \text{ mb}, \\ S_{p1}^{(0)} &= \frac{0.8007 k_{Fp}}{k_{Fn}^2} (1 + 31.28 k_{Fp} - 0.0004285 k_{Fp}^2 \\ &\quad + 26.85 k_{Fn} + 0.08012 k_{Fn}^2) (1 - 0.5898 k_{Fn} \\ &\quad + 0.2368 k_{Fn}^2 + 0.5838 k_{Fp}^2 + 0.884 k_{Fn} k_{Fp})^{-1} \text{ mb}, \\ S_{p2}^{(0)} &= \frac{0.3830 k_{Fp}^4}{k_{Fn}^{5.5}} (1 + 102.0 k_{Fp} + 53.91 k_{Fn}) \\ &\quad \times (1 - 0.7087 k_{Fn} + 0.2537 k_{Fn}^2) \end{aligned}$$

$$+ 9.404 k_{\text{Fp}}^2 - 1.589 k_{\text{Fn}} k_{\text{Fp}})^{-1} \text{ mb.} \quad (29) \quad \text{tem:}$$

The mean fit errors of  $S_{n1}^{(0)}$  and  $S_{n2}^{(0)}$  are about  $\delta_{\text{rms}} \approx 0.3\%$ , and the maximum errors  $\delta_{\text{max}} \approx 0.5\%$  take place at  $k_{\text{Fn}} \approx 1.5 \text{ fm}^{-1}$ . In the case of  $S_{p1}^{(0)}$ , we have  $\delta_{\text{rms}} \approx 1.2\%$ , with  $\delta_{\text{max}} \approx 2.9\%$  at  $k_{\text{Fn}} \approx 1.1 \text{ fm}^{-1}$  and  $k_{\text{Fp}} \approx 0.3 \text{ fm}^{-1}$ , while in the case of  $S_{p2}^{(0)}$ ,  $\delta_{\text{rms}} \approx 3.4\%$ , with  $\delta_{\text{max}} \approx 9.0\%$  at  $k_{\text{Fn}} \approx 1.1 \text{ fm}^{-1}$  and  $k_{\text{Fp}} \approx 0.4 \text{ fm}^{-1}$ .

The fits to the in-medium correction factors  $K_\alpha$  are

$$\begin{aligned} K_{n1} &= \left( \frac{m_N}{m_n^*} \right)^2 (0.4583 + 0.892 u^2 - 0.5497 u^3 \\ &\quad - 0.06205 k_{\text{Fp}} + 0.04022 k_{\text{Fp}}^2 + 0.2122 u k_{\text{Fp}}), \\ K_{n2} &= \left( \frac{m_N}{m_n^*} \right)^2 (0.4891 + 1.111 u^2 - 0.2283 u^3 \\ &\quad + 0.01589 k_{\text{Fp}} - 0.02099 k_{\text{Fp}}^2 + 0.2773 u k_{\text{Fp}}), \\ K_{p1} &= \left( \frac{m_N}{m_p^*} \right)^2 (0.04377 + 1.100 u^2 + 0.1180 u^3 \\ &\quad + 0.1626 k_{\text{Fp}} + 0.3871 u k_{\text{Fp}} - 0.2990 u^4), \\ K_{p2} &= \left( \frac{m_N}{m_p^*} \right)^2 (0.0001313 + 1.248 u^2 + 0.2403 u^3 \\ &\quad + 0.3257 k_{\text{Fp}} + 0.5536 u k_{\text{Fp}} - 0.3237 u^4 \\ &\quad + 0.09786 u^2 k_{\text{Fp}}). \end{aligned} \quad (30)$$

In the case of  $K_{n1}$  we define  $u = k_{\text{Fn}} - 1.665$ ; the mean fit error is about  $\delta_{\text{rms}} \approx 1.3\%$ , and the maximum error  $\delta_{\text{max}} \approx 3.9\%$  takes place at  $k_{\text{Fn}} \approx 1.1 \text{ fm}^{-1}$  and  $k_{\text{Fp}} \approx 0.3 \text{ fm}^{-1}$ . For  $K_{n2}$ , we have  $u = k_{\text{Fn}} - 1.556$ ,  $\delta_{\text{rms}} \approx 1.9\%$ ,  $\delta_{\text{max}} \approx 4.7\%$  at  $k_{\text{Fn}} \approx 1.8 \text{ fm}^{-1}$  and  $k_{\text{Fp}} \approx 1.2 \text{ fm}^{-1}$ . For  $K_{p1}$ , we have  $u = k_{\text{Fn}} - 2.126$ ,  $\delta_{\text{rms}} \approx 2.4\%$ ,  $\delta_{\text{max}} \approx 7.1\%$  at  $k_{\text{Fn}} \approx 1.6 \text{ fm}^{-1}$  and  $k_{\text{Fp}} \approx 1.1 \text{ fm}^{-1}$ . Finally, for  $K_{p2}$ , we have  $u = k_{\text{Fn}} - 2.116$ ,  $\delta_{\text{rms}} \approx 3.9\%$ ,  $\delta_{\text{max}} \approx 8.5\%$  at  $k_{\text{Fn}} \approx 2.1 \text{ fm}^{-1}$  and  $k_{\text{Fp}} \approx 0.5 \text{ fm}^{-1}$ .

Unfortunately, the quantities  $K_\alpha$  depend also implicitly on  $m^*$ , as the latter enters Eq. (27) for  $\epsilon_{\text{lab}}$ . For this reason, Eqs. (30) are strictly valid only if  $m_n^* = m_p^* = 0.8 m_N$ . We will use these quantities for illustration and present the final results in the form which could be modified easily if more advanced in-medium data are available.

## 2.7. Comparison with exact solution

As pointed out in Sect. 2.1, we have used the variational method while solving the kinetic equation. In principle, it is possible to derive an exact thermal conductivity, making use of the advanced theory developed by Sykes & Brooker (1970), and Højgaard Jensen et al. (1968), for one-component Fermi-systems, and extended by Flowers & Itoh (1979) and Anderson et al. (1987) to multi-component systems. In our case neutrons are the only heat carriers, and the equation which determines the energy dependence of the nonequilibrium term in the neutron distribution can be reduced to that for a one-component sys-

$$\begin{aligned} x f(x)[1 - f(x)] &= \frac{x^2 + \pi^2}{2} f(x)[1 - f(x)] \Psi(x) \\ &+ \lambda_K \int_{-\infty}^{\infty} dx_2 \frac{x + x_2}{1 - e^{-x-x_2}} f(x) f(x_2) \Psi(x_2). \end{aligned} \quad (31)$$

In this case,  $x = (\epsilon_n - \mu_n)/T$ ,  $f(x) = 1/(e^x + 1)$ , and  $\Psi(x)$  is an unknown function defined in the same fashion as in Baym & Pethick (1991). The parameter  $\lambda_K$ , originally introduced by Sykes & Brooker (1970), contains information on  $nn$  and  $np$  scattering and reads

$$\begin{aligned} \lambda_K &= \left\{ \int \frac{d\Omega (1 + 2 \cos \theta)}{\cos(\theta/2)} \mathcal{Q}_{nn}(\theta, \phi) + 8 \frac{m_p^{*2}}{m_n^{*2}} x_0 \right. \\ &\quad \times \int d\Omega [(1 + 2 x_0 \cos \theta)^2 + 4 x_0^2 \sin^2 \theta \cos \phi] \\ &\quad \times \frac{\mathcal{Q}_{np}(\theta, \phi_{\text{cm}})}{(1 + 4 x_0 \cos \theta + 4 x_0^2)^{3/2}} \left. \right\} \left[ \int \frac{d\Omega \mathcal{Q}_{nn}(\theta, \phi)}{\cos(\theta/2)} \right. \\ &\quad \left. + 8 \frac{m_p^{*2}}{m_n^{*2}} x_0 \int \frac{d\Omega \mathcal{Q}_{np}(\theta, \phi_{\text{cm}})}{(1 + 4 x_0 \cos \theta + 4 x_0^2)^{1/2}} \right]^{-1}, \end{aligned} \quad (32)$$

where  $\theta$  and  $\phi$  are Abrikosov–Khalatnikov angles,  $x_0 = k_{\text{Fp}}/(2k_{\text{Fn}})$ , and the integrations are carried out over the full solid angle ( $d\Omega = \sin \theta d\theta d\phi$ ). In the case of  $nn$  collisions,  $\phi$  is the scattering angle in the center-of-mass reference frame, while for  $np$  collisions we obtain

$$\cos \phi_{\text{cm}} = \frac{(1 - 4 x_0^2)^2 + 16 x_0^2 \sin^2 \theta \cos \phi}{(1 + 4 x_0^2)^2 - 16 x_0^2 \cos^2 \theta}. \quad (33)$$

The angle  $\theta$  is connected, in both cases, with the collision energy in laboratory reference frame (in-vacuum kinematics):

$$\epsilon_{\text{lab}} = \frac{\hbar^2}{2m_N} (k_{\text{F1}}^2 + k_{\text{F2}}^2 - 2k_{\text{F1}} k_{\text{F2}} \cos \theta). \quad (34)$$

The exact thermal conductivity of neutrons  $\kappa_{\text{exact}}$  is related to the variational thermal conductivity  $\kappa_{\text{var}}$  through the correction factor  $C$ :

$$\kappa_{\text{exact}} = \kappa_{\text{var}} C(\lambda_K), \quad C(\lambda_K) = \frac{12}{5} H(\lambda_K), \quad (35)$$

where

$$\begin{aligned} H(\lambda_K) &= \frac{3 - \lambda_K}{4} \\ &\times \sum_{n=0}^{\infty} \frac{4n + 5}{(n+1)(2n+3)[(n+1)(2n+3) - \lambda_K]} \end{aligned} \quad (36)$$

is the function introduced by Sykes & Brooker (1970). For the range of particle Fermi wave-numbers  $k_{\text{Fn}}$  and  $k_{\text{Fp}}$  considered in the present paper, the parameter  $\lambda_K$  determined from Eq. (32) varies from 0.79 to 0.97. Corresponding values of  $C(\lambda_K)$  lie between 1.20 and 1.22. It seems reasonable, therefore, to adopt the constant correction factor  $C = 1.2$  to the values of  $\kappa_{\text{var}}$ .

### 2.8. Comparison with other works

Let us compare our results with the results of several previous works at lower densities. First of all, we mention two papers by Wambach, Ainsworth & Pines (1993) (hereafter WAP) and by Sedrakian et al. (1994). WAP considered pure neutron matter at densities about  $n_0 = 0.16 \text{ fm}^{-3}$  using Landau theory. They calculated momentum dependent Landau parameters, quasiparticle transition amplitudes and transport coefficients (thermal conductivity, viscosity, and spin diffusion coefficient). As follows from their Fig. 10, panel 4 (where the quantity  $\kappa T/c$  should be expressed in  $\text{MeV}/\text{fm}^2$  rather than in  $\text{K}/\text{fm}^2$  as printed), the thermal conductivity is  $\kappa^{\text{WAP}} \approx 2 \times 10^{21} \text{ ergs s}^{-1} \text{ cm}^{-1} \text{ K}^{-1}$ , if we take  $n_n = n_0$  and  $T = 2 \text{ MeV}$ . (This particular temperature is chosen for comparison with the results of Sedrakian et al. (1994); other authors neglected temperature effect on the transition probabilities and, consequently, found the standard  $T^{-1}$  dependence of the thermal conductivity.) The value of the Landau parameter  $F_1^s$  at zero momentum transfer from WAP's Fig. 7 yields the effective mass  $m_n^* \approx 0.9m_N$  at  $n_n = n_0$ . Using our in-vacuum formula with the same  $m_n^*$  and omitting  $np$  collisions, we obtain  $\kappa \approx 2.9 \times 10^{20} \text{ ergs s}^{-1} \text{ cm}^{-1} \text{ K}^{-1}$ . With the medium effects included by using the results of Sect. 2.6 we get about  $4.7 \times 10^{20} \text{ ergs s}^{-1} \text{ cm}^{-1} \text{ K}^{-1}$ . In this case, we have taken into account rather weak dependence of the in-medium correction  $K_n$ , Eq. (30), on  $k_{\text{FP}}$ .

The calculation by Sedrakian et al. (1994), based on a thermodynamic  $T$ -matrix approach, yields  $\kappa^S \approx 2.6 \times 10^{20} \text{ ergs s}^{-1} \text{ cm}^{-1} \text{ K}^{-1}$  which agrees surprisingly well with our in-vacuum result for the same  $T=2 \text{ MeV}$  and  $n_n = n_0$ . However, the treatment of Sedrakian et al. (1994) is limited to rather high temperatures  $T > 1 \text{ MeV}$  at  $\rho \sim \rho_0$ . At lower temperatures, the authors observe a divergence of their  $nn$  scattering cross-sections indicating the onset of neutron superfluidity. It is worth noting also, that Fig. 2b of Sedrakian et al. (1994) reproduces inaccurately the thermal conductivity obtained by WAP. For instance, it gives  $2.7 \times 10^{20} \text{ ergs s}^{-1} \text{ cm}^{-1} \text{ K}^{-1}$ , for  $T$  and  $n_n$  under discussion, that is 7.5 times smaller than the actual value quoted above.

Finally, our thermal conductivity based on in-vacuum cross-sections can be directly compared with the neutron thermal conductivity obtained by Flowers & Itoh (1979). Their results are valid for a model of dense asymmetric nuclear matter proposed by Baym et al. (1971). From Fig. 1 of Flowers & Itoh (1979) we have  $\kappa_n^{\text{FI}} \approx 10^{23} \text{ ergs s}^{-1} \text{ cm}^{-1} \text{ K}^{-1}$  at  $\rho \approx 2.7 \times 10^{14} \text{ g cm}^{-3}$  and  $T = 10^8 \text{ K}$ . Corresponding particle number densities are (Baym et al., 1971)  $n_n \approx 0.153 \text{ fm}^{-3}$ , and  $n_p \approx 0.006 \text{ fm}^{-3}$ . The nucleon effective masses were taken equal to their bare masses. In this case, our formulae yield the value  $\kappa_n \approx 1.8 \times 10^{22} \text{ ergs s}^{-1} \text{ cm}^{-1} \text{ K}^{-1}$ , which is more than 5 times smaller. Note that Flowers & Itoh (1979) reported good agreement between their results obtained in two ways: from the measured vacuum phase shifts and in the spirit of Landau theory. A qualitative agreement of their results with the

Landau-theory results by WAP is clear from the above discussion. However the accuracy of their vacuum phase shift approach is questionable since  $\kappa^{\text{FI}}$  disagrees noticeably with our in-vacuum thermal conductivity. The latter is virtually exact (see Sect. 2.6) and should be the same as obtained from the measured vacuum phase shifts.

Summarizing we stress a large scatter of results obtained using various approaches. In this respect, a reliable calculation of the Landau parameters and momentum dependent quasiparticle amplitudes in the density range (2 – 3)  $\rho_0$ , at least for pure neutron and symmetrical nuclear matter, is highly desirable. It is especially true in view of relatively large discrepancies at low densities between the calculations which employ the in-vacuum cross-sections (like ours) and those performed in the frames of the Landau theory.

### 3. Effects of Superfluidity of Nucleons

The equations of Sect. 2 give the neutron thermal conductivity for non-superfluid nucleons. Now we focus on the effects of nucleon superfluidity.

It is well known (e.g., Tilley & Tilley, 1990) that the heat transport problem in superfluid matter is complicated by the appearance of convective counterflow of normal part of fluid component in the presence of a temperature gradient. Macroscopic counterflow can carry heat producing an effective thermal conductivity. A study of this effective conductivity is a delicate task which is outside the scope of the present work. We will consider the effect of superfluidity on the microscopic (diffusive) thermal conductivity. This problem is also complicated and we will adopt some model assumptions. Our consideration is basically close to that used in the studies of transport properties in superfluid  $^3\text{He}$  by Bhattacharyya et al. (1977) and Pethick et al. (1977).

It is generally believed (see, e.g., Takatsuka & Tamagaki, 1993) that the nucleon superfluidity in the neutron star cores is of the BCS type. The proton pairing occurs mainly in the singlet  $^1S_0$  state. The neutron pairing can be of the singlet type only at not too high densities,  $\rho \lesssim \rho_0$ , that is near the outer boundary of the neutron star core. At higher densities, the  $nn$  interaction in the  $^1S_0$  state becomes repulsive, and the singlet-state neutron pairing disappears. However, the  $nn$  interaction in the triplet  $^3P_2$  state is attractive, and the neutron superfluidity at densities  $\rho \gtrsim \rho_0$  is most likely to occur in this state. We consider the singlet-state proton superfluidity, and either the singlet-state or triplet-state neutron superfluidity.

Microscopically, the superfluidity leads to the appearance of an energy gap  $\delta$  in the superfluid quasiparticle dispersion relation near the Fermi surface ( $|k - k_F| \ll k_F$ ):

$$\epsilon = \text{sgn}(\xi) \sqrt{\delta^2 + \xi^2}, \quad (37)$$

where  $\xi = \hbar v_F(k - k_F)$  is the normal-state quasiparticle energy measured with respect to the chemical potential and

$v_F$  is the normal-state quasiparticle velocity at the Fermi surface. In the case of the singlet-state pairing, the energy gap  $\delta = \delta_0$  is isotropic, i.e., independent of orientation of the particle momenta with respect to a quantization axis. The temperature dependence of  $\delta_0$  can be fitted as (e.g., Levenfish & Yakovlev, 1994b)

$$y = \frac{\delta_0(T)}{T} = \sqrt{1 - \tau} \left( 1.456 - \frac{0.157}{\sqrt{\tau}} + \frac{1.764}{\tau} \right), \quad (38)$$

where  $\tau = T/T_c$  and  $T_c$  is the critical temperature.

In contrast to the isotropic singlet-state pairing, the pairing in a triplet-state produces an anisotropic gap which depends on orientation of nucleon momentum. If the direction of the quantization axis were fixed for some physical reason, this would complicate the analysis because the conductivity would be anisotropic with respect to the quantization axis. For the sake of simplicity, it is usually assumed that the orientation of the quantization axis in the neutron star cores is uncorrelated with rotational axis, temperature gradient, or magnetic field. Therefore, matter of the neutron star cores is treated as a collection of microscopic domains with arbitrary orientations of the quantization axis.

Thus we assume that the diffusive thermal conductivity is isotropic even in the presence of the triplet-state neutron pairing. Under this assumption, we may use an effective dispersion relation with an isotropic energy gap  $\delta = \delta_1$  which greatly simplifies our analysis. It would be inappropriate, though, to employ the same temperature dependence of the gap as for the singlet-state pairing gap  $\delta_0$ , Eq. (38). For instance, this would yield inaccurate gap parameters at  $T \ll T_c$ . We will take advantage of the detailed analysis by Levenfish & Yakovlev (1994a), Levenfish & Yakovlev (1994b), Yakovlev & Levenfish (1995), Yakovlev et al. (1999) of the nucleon heat capacity and various neutrino-energy loss rates in the neutron star cores for the case of triplet-state pairing of the neutrons with zero projection of the total angular momentum of Cooper pairs onto the quantization axis ( $m_J = 0$ ). According to these studies, one can obtain qualitatively accurate results using the isotropic gap  $\delta_1$  equal to the minimum value of the angle-dependent gap on the Fermi surface. The temperature dependence of this artificially isotropic gap can be fitted as (e.g., Yakovlev & Levenfish, 1995):

$$y = \frac{\delta_1(T)}{T} = \sqrt{1 - \tau} \left( 0.7893 + \frac{1.188}{\tau} \right). \quad (39)$$

Low-lying excited states of a nucleon superfluid correspond to the presence of a dilute gas of superfluid quasiparticles. The time and space evolution of the quasiparticle distribution function is governed by the transport equation. On the left-hand-side (streaming terms) there appear two terms containing derivatives of the superfluid gap but they cancel out. As a result, the left-hand-side acquires the standard form, identical to that for normal quasiparticles.

However, the collision term is, in general, more complicated than that for normal nucleon liquid. The scattering

amplitude for quasiparticles in the superfluid is a linear combination of the normal-state amplitudes. These effects were considered in detail by Bhattacharyya et al. (1977) at  $T \lesssim T_c$  and by Pethick et al. (1977) at  $T \ll T_c$  for liquid  $^3\text{He}$ . The accurate expressions for the superfluid scattering amplitudes are complicated. In view of the large uncertainty in the amplitudes even in the case of non-superfluid matter, we will keep the transition probabilities the same as in the normal case. Thus we restrict ourselves to the most important phase space effects stemming from the modification of the quasiparticle dispersion relations and resulting in a specific temperature dependence of the collision frequencies. Our results at  $T \lesssim T_c$  and  $T \ll T_c$  are in qualitative agreement with those of Bhattacharyya et al. (1977) and Pethick et al. (1977).

In order to calculate the diffusive thermal conductivity in superfluid matter we adopt the same variational approach which was used in Sect. 2 but with the modified dispersion relations, Eq. (37), containing energy gaps. In particular, the deviation function is given by the same Eq. (6), where the velocity is now given by  $v = v_F |\xi| / \sqrt{\xi^2 + \delta^2}$ . Thus, the velocity of superfluid particles varies sharply near the Fermi surface and vanishes at  $k = k_F$ .

The temperature dependences of the collision integrals can be obtained using the expressions for the energy integrals,  $J_\alpha$ , but with dispersion relations of superfluid quasiparticles. Notice that the combination of Fermi-Dirac distributions in the collision integral remains a sharp function of momenta which justifies our energy-angular decomposition (Sect. 2.3). Then from Eq. (15) we obtain

$$J_\alpha = J_\alpha^{(0)} \mathcal{R}_\alpha, \quad (40)$$

where  $J_\alpha^{(0)}$  is an energy integral (16) in non-superfluid matter and  $\mathcal{R}_\alpha$  describes the effect of nucleon superfluidity. As we use the same  $Q_{12}$  as in the normal state, the factor  $\mathcal{R}_\alpha$  represents, in our approximation, the overall effect of nucleon superfluidity on the collision integral. Our analysis shows that  $\mathcal{R}_\alpha < 1$  in the presence of neutron and/or proton superfluidity. In other words, the superfluidity always suppresses the  $nn$  and  $np$  collision frequencies. There is no discontinuity of  $\mathcal{R}_\alpha$  when a superfluidity is switched on with decreasing  $T$ . The suppression becomes very large ( $\mathcal{R}_\alpha \ll 1$ ) for strong superfluidity ( $T \gg T_c$ ).

Following Levenfish & Yakovlev (1994a) and Yakovlev & Levenfish (1995) we introduce the notations

$$x = \frac{\xi}{T}, \quad y = \frac{\delta}{T}, \quad z = \frac{\epsilon}{T} = \text{sgn}(x) \sqrt{x^2 + y^2}. \quad (41)$$

Then the correction factors for the  $np$  collisions can be written as:

$$\begin{aligned} \mathcal{R}_{p1}(y_n, y_p) &\equiv \frac{5}{2\pi^4} \int \int \int \int_{-\infty}^{+\infty} dx_n dx_p dx'_n dx'_p \\ &\quad \times \delta(z_n + z_p + z'_n + z'_p) \\ &\quad \times f(z_n) f(z_p) f(z'_n) f(z'_p) x_n^2, \\ \mathcal{R}_{p2}(y_n, y_p) &\equiv \frac{15}{2\pi^4} \int \int \int \int_{-\infty}^{+\infty} dx_n dx_p dx'_n dx'_p \end{aligned}$$



$$\begin{aligned} & \times \delta(z_n + z_p + z'_n + z'_p) \\ & \times f(z_n) f(z_p) f(z'_n) f(z'_p) (-x_n x'_n), \end{aligned} \quad (42)$$

where  $f(z) = (e^z + 1)^{-1} = 1 - f(-z)$ . The reduction factors for the  $nn$  collisions are immediately expressed through  $\mathcal{R}_{p\alpha}$ :

$$\mathcal{R}_{n\alpha}(y_n) = \mathcal{R}_{p\alpha}(y_n, y_n). \quad (43)$$

The normalization factors in Eqs. (42) are chosen to satisfy the condition  $\mathcal{R}_\alpha = 1$  for vanishing gaps. Furthermore, it is possible to analyze the asymptotic behaviour of  $\mathcal{R}_\alpha$  in the cases in which the neutron and/or proton superfluidity is strong ( $y \gg 1$ ). This can be done in the standard manner (cf. Levenfish & Yakovlev, 1994a, Levenfish & Yakovlev, 1994b, Yakovlev & Levenfish, 1995, Yakovlev et al., 1999). Let us summarize the results.

If the neutron superfluidity is strong ( $y_n \gg 1$ ), the  $nn$  collision frequency is affected by the factor

$$\mathcal{R}_{n1}(y_n) \approx \mathcal{R}_{n2}(y_n) \approx \frac{15}{4\pi^2} y_n^3 e^{-2y_n}. \quad (44)$$

In addition, we have calculated  $\mathcal{R}_{n\alpha}(y_n)$  numerically and proposed analytic fits which reproduce the numerical results and the above asymptotes:

$$\begin{aligned} \mathcal{R}_{n1}(y_n) &= \frac{2}{3} \left[ 0.9468 + \sqrt{(0.0532)^2 + 0.5346 y_n^2} \right]^3 \\ &\times \exp \left[ 0.377 - \sqrt{(0.377)^2 + 4 y_n^2} \right] \\ &+ \frac{1}{3} (1 + 1.351 y_n^2)^2 \\ &\times \exp \left[ 0.169 - \sqrt{(0.169)^2 + 9 y_n^2} \right], \\ \mathcal{R}_{n2}(y_n) &= \frac{1}{2} \left[ 0.6242 + \sqrt{(0.3758)^2 + 0.07198 y_n^2} \right]^3 \\ &\times \exp \left[ 3.6724 - \sqrt{(3.6724)^2 + 4 y_n^2} \right] \\ &+ \frac{1}{2} (1 + 0.01211 y_n^2)^9 \\ &\times \exp \left[ 7.5351 - \sqrt{(7.5351)^2 + 9 y_n^2} \right], \end{aligned} \quad (45)$$

Maximum errors of these fits do not exceed 0.5%.

Regarding  $np$  collisions, we have calculated  $\mathcal{R}_{p\alpha}(y_n, y_p)$  numerically for the cases in which either neutron or proton superfluidity is absent and fitted the numerical results by the expressions:

$$\begin{aligned} \mathcal{R}_{p1}(y_n, 0) &= \left[ 0.4459 + \sqrt{(0.5541)^2 + 0.03016 y_n^2} \right]^2 \\ &\times \exp \left[ 2.1178 - \sqrt{(2.1178)^2 + y_n^2} \right], \\ \mathcal{R}_{p2}(y_n, 0) &= \left[ 0.801 + \sqrt{(0.199)^2 + 0.04645 y_n^2} \right]^2 \\ &\times \exp \left[ 2.3569 - \sqrt{(2.3569)^2 + y_n^2} \right], \\ \mathcal{R}_{p1}(0, y_p) &= \frac{1}{2} \left[ 0.3695 + \sqrt{(0.6305)^2 + 0.01064 y_p^2} \right] \\ &\times \exp \left[ 2.4451 - \sqrt{(2.4451)^2 + y_p^2} \right] \end{aligned}$$

$$\begin{aligned} & + \frac{1}{2} (1 + 0.1917 y_p^2)^{1.4} \\ & \times \exp \left[ 4.6627 - \sqrt{(4.6627)^2 + 4 y_p^2} \right], \\ \mathcal{R}_{p2}(0, y_p) &= 0.0436 \left[ \sqrt{(4.345)^2 + 19.55 y_p^2} - 3.345 \right] \\ & \times \exp \left[ 2.0247 - \sqrt{(2.0247)^2 + y_p^2} \right] \\ & + 0.0654 \exp \left[ 8.992 - \sqrt{(8.992)^2 + 1.5 y_p^2} \right] \\ & + 0.891 \exp \left[ 9.627 - \sqrt{(9.627)^2 + 9 y_p^2} \right]. \end{aligned} \quad (46)$$

These fits reproduce numerical results calculated in the range  $y_n \leq 30$  or  $y_p \leq 30$ . The maximum fit error does not exceed 1%, 2%, 0.3%, 1.4%, respectively, and the mean fit error is about twice lower.

The most difficult is the case of  $np$  collisions in matter in which neutrons and protons are superfluid at once. In this case we have calculated  $\mathcal{R}_{p1,2}(y_n, y_p)$  numerically on a dense grid of  $y_n$  and  $y_p$  ( $y_n \leq 12$ ,  $y_p \leq 12$ ) and obtained analytic fits to these results:

$$\begin{aligned} \mathcal{R}_{p1}(y_n, y_p) &= e^{-u_+ - u_-} (0.7751 + 0.4823 u_n + 0.1124 u_p \\ &+ 0.04991 u_n^2 + 0.08513 u_n u_p + 0.01284 u_n^2 u_p) \\ &+ e^{-2u_+} (0.2249 + 0.3539 u_+ - 0.2189 u_- \\ &- 0.6069 u_n u_- + 0.7362 u_p u_+), \end{aligned} \quad (47)$$

where  $u_\beta = \sqrt{y_\beta^2 + (1.485)^2} - 1.485$ ,  $\beta = +, -, n, p$ ,  $y_- = \min(y_n, y_p)$  and  $y_+ = \max(y_n, y_p)$ . The mean fit error is about 3%, and the maximum error of 14% takes place at  $y_n \approx 10$  and  $y_p \approx 12$ , where  $\mathcal{R}_{p1}$  is exponentially small.

The fit to  $\mathcal{R}_{p2}$  reads

$$\begin{aligned} \mathcal{R}_{p2}(y_n, y_p) &= e^{-u_+ - u_-} (1.1032 + 0.8645 u_n + 0.2042 u_p \\ &+ 0.07937 u_n^2 + 0.1451 u_n u_p + 0.01333 u_n^2 u_p) \\ &+ e^{-2u_+} (-0.1032 - 0.2340 u_+ + 0.06152 u_n u_+ \\ &+ 0.7533 u_n u_- - 1.007 u_p u_+), \end{aligned} \quad (48)$$

where  $u_\beta = \sqrt{y_\beta^2 + (1.761)^2} - 1.761$  with  $\beta = +, -, n, p$ . The mean fit error is about 3.6%, and the maximum error of 14% again takes place at  $y_n \approx 10$  and  $y_p \approx 12$  where  $\mathcal{R}_{p2}$  is exponentially small. The accuracy of our fit formulae, Eqs. (47) and (48), is quite sufficient for practical applications. One can easily see that these fit formulae are in good agreement with Eqs. (45) at  $y_n = y_p$  and with Eqs. (46) either at  $y_n = 0$  or at  $y_p = 0$ .

The neutron superfluidity affects also the left-hand side of the kinetic equation given by the integral (10). For a non-superfluid matter, we obtained  $C_{n0} = k_{\text{Fn}}^3 T / (3m_n^*)$  (Sect. 2.2). In the presence of the neutron superfluidity, we can write

$$\begin{aligned} C_n(y_n) &= C_{n0} \mathcal{R}_C(y_n), \\ \mathcal{R}_C(y_n) &= \frac{6}{\pi^2} \int_0^\infty dx_n x_n^2 \frac{e^{z_n}}{(e^{z_n} - 1)^2}. \end{aligned} \quad (49)$$

In addition, the neutron superfluidity affects the neutron heat flux in Eq. (1). It turns out that this effect is described by the same factor  $\mathcal{R}_C$ . Consequently, instead of Eqs. (7) and (12) we can express the diffusive thermal conductivity in the form

$$\begin{aligned}\kappa_n &= \frac{\pi^2 T n_n \tau_n \mathcal{R}_C}{3m_n^*}, \quad \tau_n = \frac{\mathcal{R}_C}{\nu_{nn} + \nu_{np}}, \\ \nu_{12} &= \frac{2^6 m_1^* m_2^{*2} T^2}{5m_N^2 \hbar^3} S_{12}, \\ S_{nn} &= S_{n2}^{(0)} K_{n2} \mathcal{R}_{n2}(y_n) \\ &\quad + 3S_{n1}^{(0)} K_{n1} [\mathcal{R}_{n1}(y_n) - \mathcal{R}_{n2}(y_n)], \\ S_{np} &= S_{p2}^{(0)} K_{p2} \mathcal{R}_{p2}(y_n, y_p) \\ &\quad + \frac{1}{2} S_{p1}^{(0)} K_{p1} [3\mathcal{R}_{p1}(y_n, y_p) - \mathcal{R}_{p2}(y_n, y_p)].\end{aligned}\quad (50)$$

The new factor  $\mathcal{R}_C(y_n)$  is analyzed easily in the standard manner. It is equal to 1 in the absence of superfluidity, and behaves as  $\mathcal{R}_C(y_n) \approx 3\sqrt{2} (y_n/\pi)^{3/2} \exp(-y_n)$  in the limit  $y_n \rightarrow \infty$ . We have calculated this factor numerically on a dense grid of  $y_n$ . These results and the asymptotes are accurately fitted as

$$\begin{aligned}\mathcal{R}_C(y_n) &= \left[ 0.647 + \sqrt{(0.353)^2 + 0.109 y_n^2} \right]^{1.5} \\ &\quad \times \exp \left[ 1.39 - \sqrt{(1.39)^2 + y_n^2} \right].\end{aligned}\quad (51)$$

The maximum fit error does not exceed 1%.

## 4. Results and Discussion

Let us summarize the results of Sects. 2 and 3 and present practical formulae for the neutron thermal conductivity  $\kappa_n$  in the neutron star cores:

$$\begin{aligned}\kappa_n &= \frac{\pi^2 k_B^2 T n_n \tau_n \mathcal{R}_C(y_n) C}{3m_n^*} \\ &\approx 7.2 \times 10^{23} T_8 \mathcal{R}_C^2(y_n) \left( \frac{m_n}{m_n^*} \right) \\ &\quad \times \left( \frac{10^{15} \text{s}^{-1}}{\nu_{nn} + \nu_{np}} \right) \left( \frac{n_n}{n_0} \right) \text{ ergs cm}^{-1} \text{ s}^{-1} \text{ K}^{-1}.\end{aligned}\quad (52)$$

Here,  $n_0 = 0.16 \text{ fm}^{-3}$  is the normal nucleon density,  $T_8$  is temperature in units of  $10^8 \text{ K}$ ,  $k_B$  is the Boltzmann constant (now presented explicitly),  $C=1.2$  is the correction factor discussed in Sect. 2.7;  $\mathcal{R}_C(y_n)$  is the superfluid reduction factor. The latter factor depends on the neutron gap parameter  $y_n$  and is given by Eq. (51). The gap parameter  $y_n$  is determined either by Eq. (38) for singlet-state neutron pairing or by Eq. (39) for triplet-state neutron pairing as explained in Sect. 3. Let us remind that we consider the diffusive thermal conductivity and do not analyse convective heat transport in superfluid matter.

According to Eqs. (21) and (40), the  $nn$  and  $np$  collision frequencies in Eq. (52) are

$$\nu_{nn} = \frac{2^6 m_n^* k_B^2 T^2}{5m_N^2 \hbar^3} S_{nn} \approx 3.48 \times 10^{15} \left( \frac{m_n}{m_n^*} \right)^3 T_8^2$$

$$\begin{aligned}&\times \left\{ S_{n2}^{(0)} K_{n2} \mathcal{R}_{n2}(y_n) \right. \\ &\quad \left. + 3S_{n1}^{(0)} K_{n1} [\mathcal{R}_{n1}(y_n) - \mathcal{R}_{n2}(y_n)] \right\} \text{ s}^{-1}, \\ \nu_{np} &= \frac{2^6 m_n^* m_p^{*2} k_B^2 T^2}{5m_N^2 \hbar^3} S_{np} \\ &\approx 3.48 \times 10^{15} \left( \frac{m_n}{m_n^*} \right) \left( \frac{m_p}{m_p^*} \right)^2 T_8^2 \\ &\quad \times \left\{ S_{p2}^{(0)} K_{p2} \mathcal{R}_{p2}(y_n, y_p) + 0.5 K_{p1} \right. \\ &\quad \left. \times S_{p1}^{(0)} [3\mathcal{R}_{p1}(y_n, y_p) - \mathcal{R}_{p2}(y_n, y_p)] \right\} \text{ s}^{-1}.\end{aligned}\quad (53)$$

Here,  $S_\alpha^{(0)}$  ( $\alpha = n1, n2, p1, p2$ ) is a normalized transition probability integrated over momentum transfers of colliding particles (Sects. 2.4–2.6) for free nucleons [expressed in mb and fitted by Eqs. (29)];  $K_\alpha$  describes the in-medium effects on the squared matrix element [the fits are given by Eqs. (30)];  $\mathcal{R}_\alpha$  is a corresponding superfluid reduction factor whose fits are given by Eqs. (45)–(48). Thus we obtained a simple description of the diffusive neutron conductivity in the density range from  $0.5\rho_0$  to  $3\rho_0$  (see Sect. 2). Although we have employed the Bonn model of  $NN$  interaction, we hope that the results could be used, at least semi-quantitatively, for a wide class of equations of state if one takes effective nucleon masses  $m_N^*$ , Fermi momenta  $k_{FN}$ , and superfluid gaps appropriate to these equations of state. Moreover, our results are presented in the form which enables one to include the in-medium effects from more elaborated (future) calculations of the nucleon quasi-particle transition probabilities. It would be sufficient to recalculate four in-medium correction factors  $K_\alpha$  [defined in Eq. (28)] while all other quantities in Eqs. (52)–(53) will remain untouched.

The results are illustrated in Figs. 1–4. Figure 1 presents the neutron thermal conductivity versus density at  $T = 5 \times 10^8 \text{ K}$  for non-superfluid matter. Here, we use the simplified model of free degenerate neutrons, protons and electrons (e.g., Shapiro & Teukolsky, 1983). This model yields an extremely soft equation of state, with very low fraction (about 0.6% at  $\rho = \rho_0$ ) of protons and electrons. The effective masses of nucleons are set equal to their bare masses, and no in-medium effects are included in the  $nn$  and  $np$  collision frequencies. The solid curve depicts the full neutron conductivity, which takes account of  $nn$  and  $np$  collisions. The dashed line shows the contribution from  $nn$  collisions alone. The  $nn$  and  $np$  collisions are seen to be of comparable importance despite the extreme smallness of the proton fraction. This is related to the fact that the  $np$  collisions occur at smaller laboratory energies and scattering angles than the  $nn$  ones, while the  $NN$  differential cross sections tend to grow with decrease of both these parameters. We present also the electron conductivity (the dotted line) calculated using the results of Gnedin & Yakovlev (1995).

Figure 2 demonstrates the significance of in-medium effects. It displays the ratios of in-medium to in-vacuum  $nN$  collision frequencies versus Fermi wavenumber of neu-

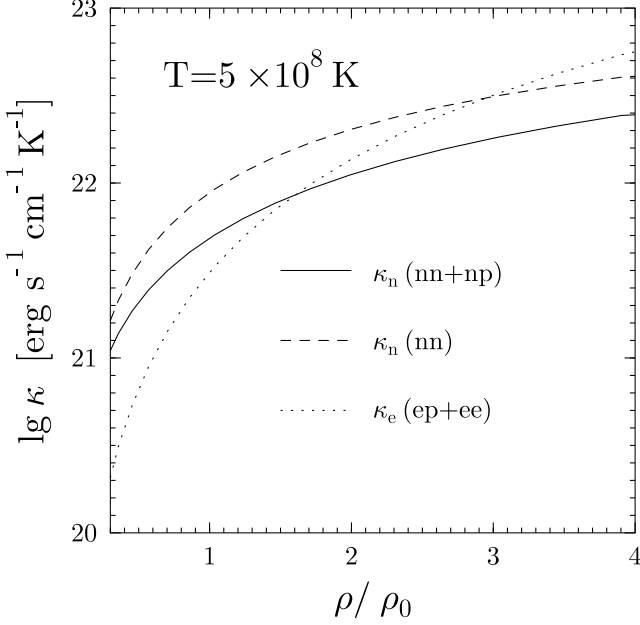


**Fig. 1.** Thermal conductivity of neutrons and electrons versus mass density (in units of  $\rho_0 = 2.8 \times 10^{14} \text{ g cm}^{-3}$ ) of non-superfluid  $npe$  matter in the model of free particles at  $T = 5 \times 10^8 \text{ K}$ ;  $m_N^* = m_N$ .

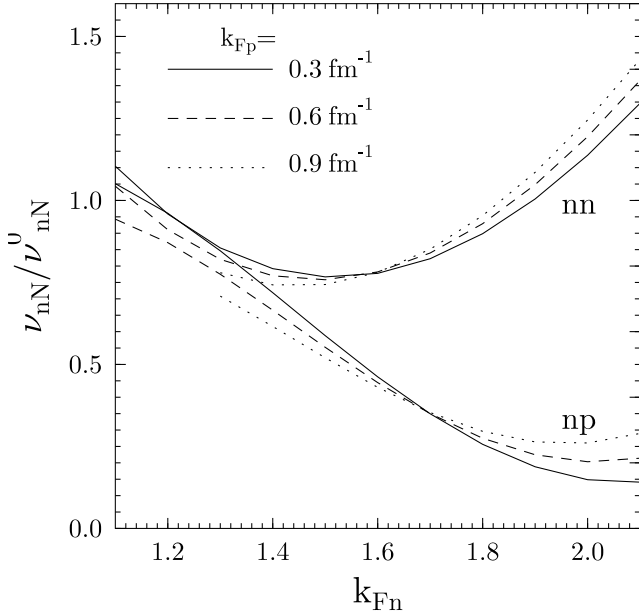


**Fig. 2.** Ratios of in-medium to in-vacuum  $nn$  and  $np$  collision frequencies versus  $k_{Fn}$  at  $k_{Fp} = 0.3 \text{ fm}^{-1}$  (solid lines),  $0.6 \text{ fm}^{-1}$  (dashes) and  $0.9 \text{ fm}^{-1}$  (dots);  $m_N^* = 0.8 m_N$ .

trons  $k_{Fn}$  (notice that  $k_{Fn} \approx 1.7 \text{ fm}^{-1}$  at  $\rho = \rho_0$ ) at three values of the proton Fermi wavenumber,  $k_{Fp} = 0.3, 0.6$  and  $0.9 \text{ fm}^{-1}$ . Let us emphasize again that we use one particular model of  $NV$  interaction in medium which is valid, strictly speaking, for symmetric nuclear matter as

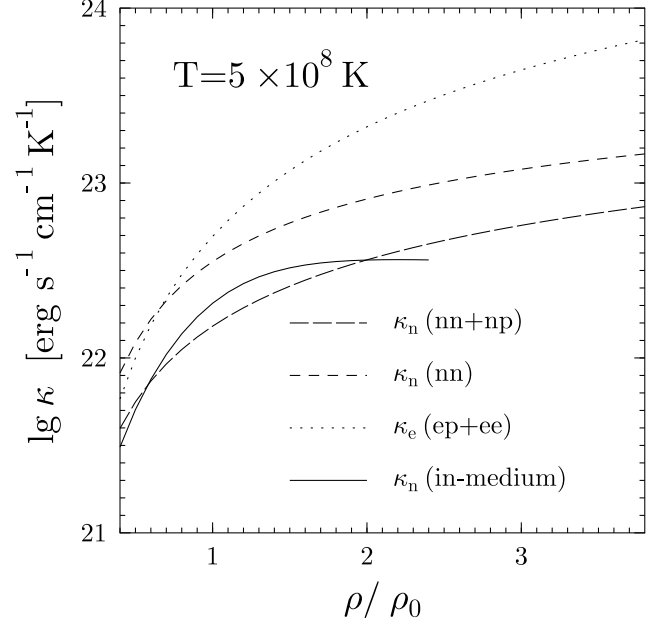


**Fig. 3.** Thermal conductivity of neutrons and electrons versus mass density in non-superfluid  $npe$  matter with a moderately stiff equation of state (Prakash et al., 1988, Page & Applegate, 1992),  $m_N^* = 0.7 m_N$  at  $T = 5 \times 10^8 \text{ K}$ . Solid curve is calculated with the in-medium  $nn$  and  $np$  scattering cross sections while other neutron-conductivity curves are obtained with the in-vacuum cross sections.

described in Sect. 2.6. The in-medium effects are seen to be significant, especially for  $np$  collisions, and determined mostly by  $k_{Fn}$ . For instance, at  $k_{Fn} \approx 2 \text{ fm}^{-1}$  the in-medium effects reduce  $\nu_{np}$  by a factor of 3–6. The dependence of the ratios in question on the proton fraction (on  $k_{Fp}$ ) appears rather weak.

Figure 3 shows the neutron and electron thermal conductivities versus density at  $T = 5 \times 10^8 \text{ K}$  for non-superfluid matter described by a moderately stiff equation of state proposed by Prakash et al. (1988) [the version with the compression modulus  $K_0 = 180 \text{ MeV}$ , and the same model function  $F(u)$  as in Page & Applegate (1992)]. This equation of state is much more realistic than the model of free particles employed in Fig. 1; it yields much larger fractions of protons and electrons (e.g., about 6% at  $\rho = \rho_0$ ). The effective nucleon masses are put equal to  $0.7 m_N$ . The solid curve takes into account the contribution from  $nn$  and  $np$  collision frequencies evaluated with the in-medium cross sections (Fig. 2). The curve is plotted up to  $\rho \approx 3 \rho_0$ , in the density range where the in-medium scattering cross sections are available (Sect. 2.6). Other neutron-conductivity curves are calculated with the in-vacuum cross sections [ $K_\alpha = 1$  in Eqs. (53)]. In contrast to Fig. 1, the electron thermal conductivity exceeds the neutron one at all densities, which is explained by the much higher fraction of electrons for the adopted equation of state. Comparing Figs. 1 and 3 one can deduce that the electron conductivity is more sensitive to the equation of

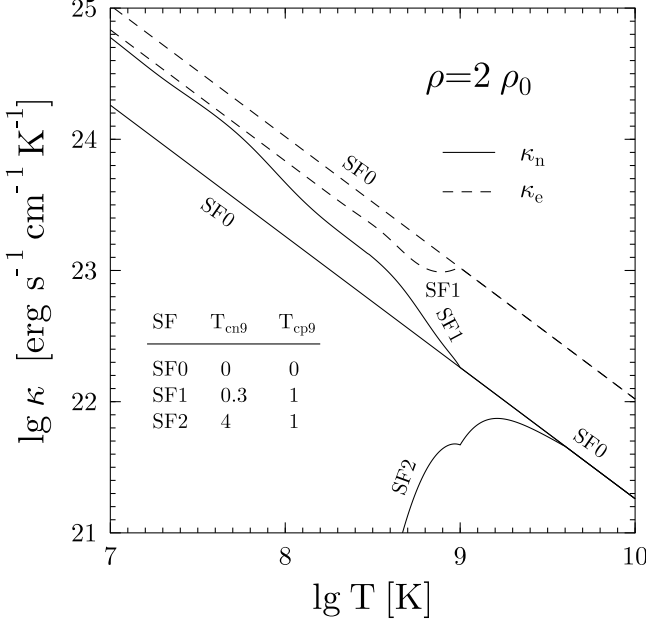


**Fig. 4.** Diffusive thermal conductivity of neutrons (solid lines) and electrons (dashes) versus temperature at  $\rho = 2\rho_0$  for the same equation of state as in Fig. 3. The curves marked SF0 refer to the non-superfluid case; the curves marked SF1 imply  $T_{cn} = 3 \times 10^8$  K,  $T_{cp} = 10^9$  K, while the curve SF2 corresponds to  $T_{cn} = 4 \times 10^9$  K,  $T_{cp} = 10^9$  K (singlet-state proton and triplet-state neutron superfluidities). The in-medium effects in the scattering cross sections are not included. The dashed curve SF1 is equally valid for the case SF2.

state than the neutron one. This is because the number density of electrons varies more strongly with the equation of state than the number density of neutrons. In fact, the variation of the neutron conductivity is mostly caused by the difference in effective nucleon masses between the two models.

Finally, Fig. 4 demonstrates the effects of neutron and proton superfluidity. It shows the temperature dependence of the diffusive thermal conductivity for the same model of matter as in Fig. 3 at  $\rho = 2\rho_0$ . Solid and dashed lines display the neutron and electron thermal conductivity, respectively. The curves marked as SF0 correspond to non-superfluid matter; the curves SF1 correspond to the model in which  $T_{cn} = 3 \times 10^8$  K,  $T_{cp} = 10^9$  K, i.e., the proton superfluidity is stronger than the neutron one. Finally, the curve SF2 is for the case  $T_{cn} = 4 \times 10^9$  K,  $T_{cp} = 10^9$  K, in which the neutron superfluidity is stronger. The proton superfluidity is assumed to be of singlet type [the dependence of the gap on the temperature is given by Eq. (38)] while the superfluidity of neutrons is taken to be of triplet type with the gap made artificially independent of the direction of particle momentum [the temperature dependence of the gap is given by Eq. (39)]. Note that the electron thermal conductivity is independent of superfluid state of neutrons and is the same for models SF1 and SF2.

All the solid curves are obtained with in-vacuum cross sections. In the absence of superfluidity, both conductivities,  $\kappa_n$  and  $\kappa_e$ , behave as  $T^{-1}$ . When temperature falls below  $T_{cn}$  or  $T_{cp}$ , the conductivity depends on  $T$  in a more complicated manner.

If  $T_{cn} > T_{cp}$  (curve SF2, dashed curve SF1 is equally valid for the superfluid model SF2), and the temperature falls below  $T_{cn}$  the electron conductivity remains unaffected but the diffusive neutron thermal conductivity drops exponentially due to sharp decrease of the density of heat carriers — neutron quasiparticles whose momenta are sufficiently close to the neutron Fermi momentum. When  $T$  falls below  $T_{cp}$  the electron thermal conductivity undergoes a slight reduction associated mainly with variation in the plasma screening length (the proton screening which is efficient at  $T > T_{cp}$  dies out leaving alone the weaker electron screening).

If  $T_{cp} > T_{cn}$  (curves SF1), the proton superfluidity occurs first with decreasing  $T$ . It switches off the  $np$  collisions and thus enhances  $\kappa_n$ . When the temperature reaches  $T_{cn}$ , the neutron conductivity continues to grow over the non-superfluid one. At further decrease of  $T$  the neutron conductivity is determined by competition of two factors: the suppression due to the decline of the density of the heat carriers, and the enhancement due to lowering the  $nn$  collision frequency (while the  $np$  collisions are almost switched off). If  $T \ll T_{cn}$  both factors nearly cancel each other out, and the conductivity, although deviates somewhat from the non-superfluid one, but reproduces the standard temperature dependence  $T^{-1}$ . Analogous effect was demonstrated by Pethick et al. (1977) in the case of superfluid  ${}^3\text{He}$  at  $T \ll T_c$ .

We see that the nucleon superfluidity affects the neutron thermal conductivity in different ways, producing either enhancement or suppression, which is incorporated easily in computations using Eqs. (52) and (53).

We have considered thermal conductivity of matter composed of neutrons, protons, electrons, and muons at  $\rho \sim \rho_0$ . Let us discuss briefly thermal conductivity in hyperonic matter which may appear at higher  $\rho$  (e.g., Balberg et al. 1999). It may contain  $\Sigma^-$ ,  $\Lambda$  and other hyperons. Theoretical knowledge of hyperon interaction is rather uncertain but numerous models of hyperonic matter give qualitatively the same results.  $\Sigma^-$  and  $\Lambda$  hyperons appear at about the same density. Their relative fractions increase sharply with growing  $\rho$  while the fractions of electrons and muons become much lower than in the absence of hyperons. The fraction of  $\Lambda$  hyperons is typically larger than that of  $\Sigma^-$  hyperons. Qualitatively, electrons and muons are replaced by  $\Sigma^-$  hyperons while neutrons are partially replaced by  $\Lambda$  hyperons. Both replacements have important consequences for thermal conduction.

It is likely that thermal conductivities limited by Coulomb and nuclear interactions will remain decoupled. Lowering the electron and muon fractions reduces the efficiency of the electron and muon Coulomb thermal conductivities. These conductivities can be determined easily using the results of Gnedin & Yakovlev (1995). On the

other hand, the efficiency of thermal conductivity, limited by strong interactions, becomes higher. Neutrons and  $\Lambda$  hyperons may become the main heat carriers of comparable importance. Their thermal conductivity will be determined by collisions of these particles with themselves and with other strongly interacting particles (protons,  $\Sigma^-$ , etc.). Their effective collision frequencies are likely to be coupled. The theory of thermal conductivity of neutrons and  $\Lambda$  hyperons may be constructed using the formalism of Flowers & Itoh (1979) and Anderson et al. (1987). The main problem would be to calculate the scattering cross sections of strongly interacting particles of various species taking into account many-body effects. Hyperons, like nucleons, may be in superfluid state (e.g., Balberg et al. 1999) forming multicomponent superfluid. The effects of superfluidity on the diffusive thermal conductivity can be included in the same manner as in Sect. 3. Consideration of convective heat transport would be even more complicated than in nucleon matter (see above). Therefore, thermal conduction in hyperonic matter remains an open problem. It deserves a separate study which goes far beyond the scope of present paper.

## 5. Conclusions

We have calculated the thermal conductivity of neutrons due to  $nn$  and  $np$  collisions in the neutron star cores. The results are valid for densities  $\rho$  from  $0.5\rho_0$  to  $3\rho_0$  (see Sect. 2). We have included the effects of possible superfluidity of neutrons and protons (Sect. 3) and obtained practical expressions (Sect. 4) for the diffusive thermal conductivity valid for a wide class of models of dense matter. The results can be generalized to the case in which hyperons are present in dense matter along with nucleons.

Our results, combined with those of Gnedin & Yakovlev (1995) for the electron thermal conductivity, provide a description of the transport properties in the neutron star cores. This thermal conductivity is needed for numerical simulations of cooling of young neutron stars with non-isothermal core (age up to 10 – 100 years).

*Acknowledgements.* We are grateful to A.D. Kaminker and D.A. Varshalovich for useful comments, to V.A. Kudryavtsev for fruitful discussions, and also to R. Machleidt and G.Q. Li for providing us with the  $NN$  scattering cross sections. We acknowledge useful remark of anonymous referee. Two of us (DAB and DGY) are pleased to acknowledge excellent working conditions at Copernicus Astronomical Center, Warsaw. This work was supported in part by the RFBR (grant No. 99-02-18099), INTAS (grant No. 96-0542), KBN (grant No. 2 P 03D 01413), and NSF (grant No. PHY99-07949).

## References

- Anderson R.H., Pethick C.J., Quader K.F., 1987, Phys. Rev. B35, 1620  
 Balberg B., Lichtenstadt I., Cook G.B., 1999, ApJS 121, 515  
 Baym G., Bethe H.A., Pethick C.J., 1971, Nucl. Phys. A175, 225  
 Baym G., Pethick C., 1991, Landau Fermi–Liquid Theory, John Wiley, New York  
 Bhattacharyya P., Pethick C.J., Smith H., 1977, Phys. Rev. B15, 3367  
 Flowers E., Itoh N., 1979, ApJ 230, 847  
 Flowers E., Itoh N., 1981 ApJ 250, 750  
 Gnedin O.Y., Yakovlev D.G., 1995, Nucl. Phys. A582, 697  
 Højgaard Jensen H., Smith H., Wilkins J.W., 1968, Phys. Lett. A27, 532; 1969, Phys. Rev. 185, 323  
 Lattimer J.M., Van Riper K.A., Prakash M., Prakash M., 1994, ApJ 425, 802  
 Levenfish K.P., Yakovlev D.G., 1994, Astron. Lett. 20, 43  
 Levenfish K.P., Yakovlev D.G., 1994, Astron. Rep. 38, 247  
 Li G.Q., Machleidt R., 1993, Phys. Rev. C48, 1702  
 Li G.Q., Machleidt R., 1994, Phys. Rev. C49, 566  
 Lorenz C.P., Ravenhall D.G., Pethick C.J., 1993, Phys. Rev. Lett. 70, 379  
 Machleidt R., Holinde K., Elster Ch., 1987, Phys. Rep. 149, 1  
 Page D., Applegate J.H., 1992, ApJ 394, L17  
 Pethick C.J., Smith H., Bhattacharyya P., 1977, Phys. Rev. B15, 3384  
 Pethick C.J., Ravenhall D.G., 1995, Ann. Rev. Nucl. Particle Sci. 45, 429  
 Pines D., 1991. In: J. Ventura and D. Pines (eds.) Neutron Stars: Theory and Observation. Kluwer Academic Publisher, Dordrecht p. 57,  
 Prakash M., Ainsworth T.L., Lattimer J.M., 1988, Phys. Rev. Lett. 61, 2518  
 Sedrakian A.D., Blaschke D., Röpke G., Schulz H., 1994, Phys. Lett. B338, 111  
 Shapiro S.L., Teukolsky S.A., 1983, Black Holes, White Dwarfs, and Neutron Stars, Wiley-Interscience, New York  
 Sykes J., Brooker G.A., 1970, Ann. Phys. 56, 1  
 Takatsuka T., Tamagaki R., 1993, Progr. Theor. Phys. Suppl. 112, 27  
 Tilley D.R., Tilley J., 1990, Superfluidity and Superconductivity, IOP Publishing, Bristol  
 Umeda H., Shibasaki N., Nomoto K., Tsuruta S., 1993, ApJ 408, 186  
 Van Riper K.A., 1991, ApJS 75, 449  
 Wambach J., Ainsworth T.L., Pines D., 1993, Nucl. Phys. A555, 128 (WAP)  
 Yakovlev D.G., Levenfish K.P., 1995, A&A 297, 717  
 Yakovlev D.G., Levenfish K.P., Shibano Yu.A., 1999, Physics–Uspekhi 42, 737  
 Ziman J.M., 1960, Electrons and Phonons, Oxford University Press, Oxford